

# VIBRATION AND IMPACT DETECTION OF AXIAL- FLOW THRESHING UNIT UNDER DYNAMIC THRESHING CONDITIONS

## 动态脱粒工况下轴流脱粒装置的振动与冲击检测

Ji Jiangtao<sup>1,2)</sup>, Hu Jingpeng<sup>1)</sup>, Wang Shengsheng<sup>1,2)</sup>, Zhang Ruihong<sup>1)</sup>, Pang Jing<sup>1)</sup> <sup>1</sup>

<sup>1)</sup> Henan University of Science and Technology, College of Agricultural Equipment Engineering/ China;

<sup>2)</sup> Collaborative Innovation Centre of Machinery Equipment Advanced Manufacturing of Henan Province/ China

Tel: +86-379-64877837; E-mail: jjt0907@163.com

DOI: <https://doi.org/10.35633/inmateh-60-21>

**Keywords:** Axial-flow threshing unit; vibration; impact; acceleration; stress

### ABSTRACT

In order to explore the interaction between the axial-flow threshing unit and the agricultural materials, the vibration signal of the axial-flow threshing unit and the stress signal of the internal threshing tooth under the dynamic threshing condition were detected by using the three-way acceleration sensors and the resistance strain gauges. The results show that under the dynamic threshing condition, the amplitude of the vibration signal along the axial direction of the threshing unit experienced a small change, but changed greatly at the feeding direction of materials and vertical direction of fixed bearings, which was mainly caused by the internal impact between the threshing unit and the materials; Under the impact of materials, the threshing element of each measuring point has a continuous peak value of stress signal, and the stress signals gradually decreased along the axial direction. This study further reveals the interaction mechanism between axial-flow threshing unit and materials from the perspective of vibration and impact, and provides new methods for the development of condition detection technology of grain harvesting equipment.

### 摘要

脱粒装置内部与物料作用情况极其复杂, 为探究轴流脱粒装置与物料之间的相互作用情况, 采用三向加速度传感器和电阻应变片, 实现了动态脱粒工况下轴流脱粒滚筒的振动信号及内部脱粒元件的应力信号的检测。结果表明: 轴流脱粒滚筒由空转变化至脱粒工况, 沿物料轴向运动方向振动幅值变化较小, 沿物料喂入方向和轴承座上下方向的振动幅值变化较为明显; 各测点脱粒元件受冲击载荷作用而出现连续的应力峰值, 且大小沿轴向逐渐降低。本研究从振动和冲击应力的角度进一步揭示了轴流脱粒装置与物料之间的相互作用机理, 为谷物收获装备工况检测技术的发展提供了新的方法和思路。

### INTRODUCTION

Axial-flow threshing unit is one of the commonly used threshing forms of the current harvesting equipment (Bello B et al, 2019). Spike tooth is the most widely used threshing element, and it completes the threshing and separating function by impact with the threshed object. The mechanical state of the materials in the threshing unit directly affects the quality of threshing process. Therefore, to improve the threshing quality, it is one of the important contents to develop the mechanism of the interaction between the axial-flow threshing unit and the materials.

Domestic and foreign scholars have focused on the research of the interaction mechanism between the threshing units and materials, mainly about the construction of mathematical models and simulation tests, and most of these works were based on some assumptions, which were quite different from the actual working process of the threshing unit (Chansrakoo and Chuan-Udom, 2018; Steponavicius D et al, 2018; Miu P. and Kutzbach H., 2008). During the actual working process, the threshing unit generated vibration and impact response due to the reaction force of the materials. Tang Zhong et al. reached the conclusion that the unbalanced vibration of the tangential-flow threshing unit was caused by the threshing load by comparing the amplitude of the cutting-flow threshing unit under the condition of idling and threshing (Tang Zhong et al., 2019). Hamed et al carried out dynamic modeling and vibration analysis on the rasp-bar of tangential-flow thresher, and improved the vibration phenomenon by optimizing the structure of the threshing machine (Zare H. et al, 2019).

<sup>1</sup> Ji Jiangtao, Prof. Ph.D. Eng.; Hu Jingpeng, Wang Shengsheng, Ph.D. Eng., Zhang Ruihong, Pang Jing

Therefore, it is necessary to study the vibration phenomenon of the axial-flow threshing unit in threshing process. Wang Yue et al. analysed and calculated the impact frequency and impact stress of the crop in the axial-flow threshing unit, and explained the mechanism of stem and leaf fracture from the perspective of stress (Wang Yue and Ma Ji, 1987). Xie Fangping et al. designed a threshing unit with flexible-spike tooth based on the theory of energy conservation, and simulated the deformation and stress distribution of the flexible-spike tooth under threshing load. The simulation results show that the maximum deformation of the threshing tooth occurred at the free end, and the maximum stress generated at the fixed end (Xie Fangping et al, 2009). The above research shows that it is feasible to use the impact stress of threshing elements to characterize the impact degree of materials, but it is still at the theoretical level, and there is no relevant report on the detection of impact stress at present.

The internal threshing space is complicated and narrow to fix the detection devices in the axial-flow threshing unit. To solve these problems, we set up a vibration and impact detection system on the test bench of axial-flow threshing unit and completed the real-time detection of the vibration signal of the axial-flow threshing unit and the impact stress signal of the spike tooth, which provides new methods for the development of condition detection technology of grain harvesting equipment.

## MATERIALS AND METHODS

### CONSTRUCTION OF DETECTION SYSTEM OF VIBRATION AND IMPACT

#### Composition of vibration and impact test bench

The test bench is mainly composed of an axial-flow threshing unit and a detection system, as shown in Fig. 1, which is used to collect the vibration signal of the threshing unit and the stress signal of the spike tooth in real time. The material was fed through the feeding inlet, and it moved in a spiral direction along the threshing cylinder under the impact and friction of the spike tooth. The seeds were continuously removed, collected by the collecting device, and the remaining stalks were discharged from the grass discharge.

The vibration and impact detection system consisted of a three-axis acceleration sensor, resistance strain gauges, Robust DH5902 dynamic signal acquisition instrument and DH5905 wireless telemetry analysis system. The vibration signal was measured by the three-axis accelerometer (356A16). The stress signal was measured by the resistance strain gauges. The performance parameters of the DH5902 dynamic signal acquisition instrument, DH5905 wireless telemetry system and sensors are shown in Tab.1.

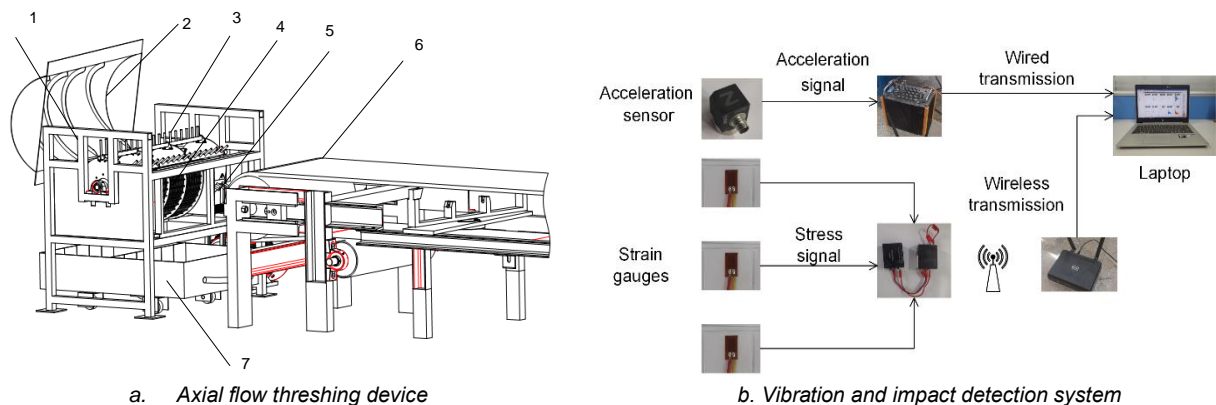


**Fig. 1 -Test bench for vibration and impact testing**

1. Frame; 2. Top cover; 3. Axial-flow threshing cylinder; 4. Concave plate; 5. Feeding inlet;  
6. Conveying device; 7. Collecting device

### DETECTION PRINCIPLE OF VIBRATION AND IMPACT

#### Vibration detection of axial flow threshing drum

When the conveying device works continuously, there is an interaction between the materials and the threshing cylinder. The spike tooth is arranged in the form of spiral along the axial direction, which is in direct contact with the materials. And the reverse force from the materials on each spike tooth is  $F_i$ . In every revolution of the threshing process, only some of the spike teeth are in direct contact with the materials, and the whole threshing cylinder is subjected to eccentric load. The force diagram is shown in Fig. 2.

The reverse force  $F_i$  can be decomposed into components  $F_{iy}$  and  $F_{iz}$  in the horizontal and vertical directions, the axial force  $F_{ix}$  comes from the axial push of the top cover on the materials. According to the knowledge of mechanical vibration, the reverse force of the material flow on the cylinder can be used as an external excitation force, which can cause the unbalanced vibration of the threshing cylinder. The axial-flow threshing cylinder is matched with the bearing and fixed to the frame by bolts. According to references (Syuhri A et al, 2018), the bearings can be simplified to springs ( $K_B$ ) and damping ( $C_B$ ), and the cylinder itself is treated as a spring ( $K_{EQ}$ ), there by the entire physical model can be simplified and transformed into a series connection of the bearing and the threshing cylinder, as shown in Fig. 2. Therefore, the vibration of the bearing can be used to represent the vibration of the entire threshing cylinder.

Table 1-

Performance parameters of vibration impact detection system		
Name	Performance indicator	Parameter value
Dynamic signal acquisition instrument (DH5902)	Number of channels	16
	Highest sampling frequency [KHz]	100
	Distortion [%FS]	<0.5
Wireless telemetry system (DH5905)	Wireless mode	Wi-Fi
	Highest sampling frequency [KHz]	4
	A/D conversion[system]	16
Accelerometer (356A16)	Range [g]	±50
	Frequency response [Hz]	0.3~6000
	Sensitivity [ $mV \cdot g^{-1}$ ]	100
	Lateral sensitivity [%]	<5
Resistance strain gauge (120-3AA)	Resistance [ $\Omega$ ]	120
	Sensitivity [ $mV \cdot V^{-1}$ ]	2.0
	Base size [mm]	6.9*3.9
	Wire grid size [mm]	3.0*2.3

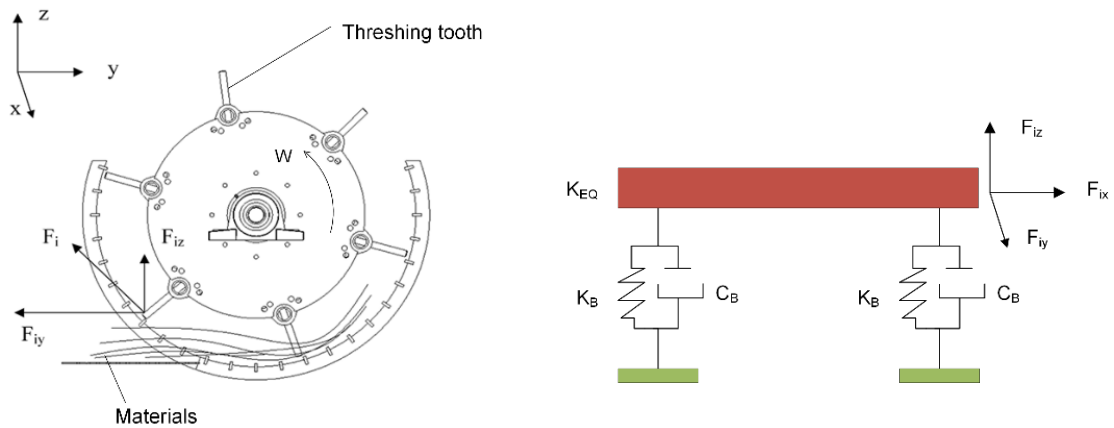


Fig. 2 - Schematic diagram force and vibration model

The amplitude of vibration detected from the bearing of the threshing cylinder in three directions can evaluate the interaction between the axial threshing cylinder and the materials. For easy description of the directions of vibration, a coordinate system is set on the axial-flow threshing cylinder. The X direction indicates the axial direction of the threshing cylinder. The Y direction indicates the tangential direction of the threshing cylinder, and the Z direction indicates the vertical direction of bearing pedestal. The three-axis accelerometer is used to measure the vibration signals in the three directions above, and the sensor is placed above the vertical bearing by the magnetic seat. The actual installation position of the three-axis accelerometer is shown in Figure 3. During the dynamic threshing process, in order to reduce the interference caused by the shaking of the connecting wire during the detection, the connecting wire is fixed by tape.

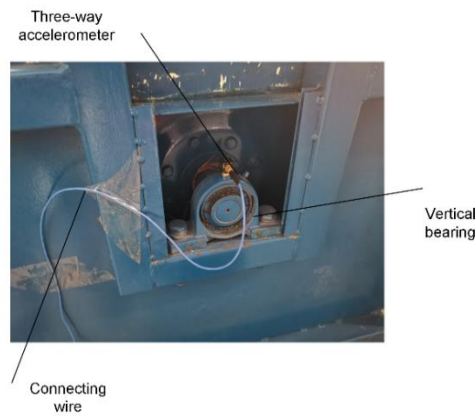


Fig. 3 - Installation position of the accelerometer sensor

**Detection of impact stress**

The impact load between the materials and the threshing unit causes the unbalanced vibration of the threshing cylinder, which can roughly describe the interaction inside the unit. And the threshing elements, which are in direct contact with the materials, can reflect the interaction mechanism between the material and the spike tooth during the threshing process (Tang Zhong et al, 2019). However, there are no measuring reports about the impact stress of threshing elements at present.

Without considering the influence of the interaction force and the friction force among the materials, we suppose the interaction between the spike tooth and the materials conforms to the law of conservation of energy and the theorem of impulse.

$$F^* = \frac{1}{\tau} \int_0^\tau F dt = \frac{mg(v_2 - v_1)}{\tau} \tag{1}$$

Where:

$V_2$  is the speed of the materials, [m/s];  $V_1$  is the speed of the spike tooth, [m/s];  $F$  is the interaction force between the materials and the spike tooth, [N];  $F^*$  is the average force on the spike tooth from the materials, [N];  $\tau$  is the contact time between the materials and the spike tooth, [s].

The spike teeth are all fixed with the gear rod during threshing process, and only the spike tooth interacts with the materials. Based on the theory of cantilever beam in mechanics of materials, each threshing tooth can be simplified as a cantilever beam model, as shown in Fig. 4.

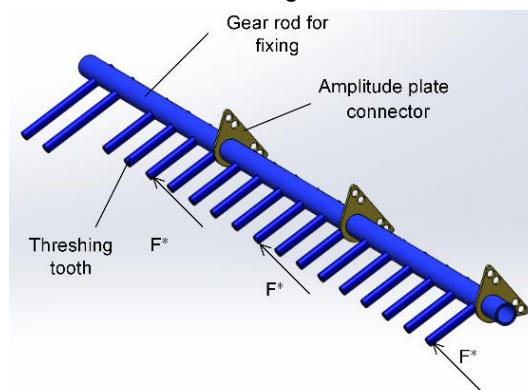


Fig. 4 - Simplified force diagram of the cantilever beam with spike teeth

The spike tooth will generate mechanical stress and strain under the impact load of the materials. The stress signal can be measured by the strain gauge and collected by the DH5905 dynamic signal acquisition instrument. It can be known from the material mechanics that the type of impact stress generated inside the spike teeth belongs to the kind of bending normal stress (Xie Fangping et al., 2009), and the formula for calculating the maximum bending normal stress is:

$$\delta_{\max} = \frac{M_{\max}}{W_z} = \frac{F^* l}{W_z} = \frac{mg \cdot \Delta v \cdot l}{\tau \cdot W_z} \tag{2}$$

Where:

$\delta_{max}$  is the maximum bending normal stress of the spike tooth, [MPa];  $M_{max}$  is the maximum bending moment generated by the impact load, [MPa];  $l$  is the equivalent length of the spike tooth, [mm];  $W_z$  is the modulus of flexural section of the spike tooth, [mm<sup>3</sup>]. It can be known from formula (2) that the impact load of the spike tooth is related to the mass, speed and collision position of the materials.

The maximum bending stress of the spike tooth is usually produced near the fixed end. (Xie Fangping et al., 2009). According to the preliminary tests, if the strain gauge was pasted near the top of the spike tooth, the probability of the strain gauge contacting the materials directly would increase, resulting in the abnormal peak value of the impact stress signal. Once the strain gauge was damaged under the impact of materials, the test couldn't be carried out. Therefore, in order to ensure that a reasonable stress signal can be detected and the strain gauge is protected from damage, the strain gauge should be placed close to the root of the spike tooth. To further ensure the normal arrangement of the terminals and leads of the strain gauges, it was finally determined that the strain gauge was attached at a position of 10 mm away from the root of the spike tooth. The sticking method of the strain gauge adopts a 1/2 Wheatstone bridge, that is, two pieces are attached to the front and the back of the spike tooth respectively, and this method is only suitable for measuring the bending strain, eliminating the stretching and the compressive strain, which conforms to the deformation law under the normal stress of the spike tooth (Li Yaoming et al., 2013), as shown in Fig. 5a.

After the sticking was completed, one ohmmeter was used to check the quality of the strain gauges. The unqualified strain gauges should be replaced in time. And finally, the protective rubber was applied on the surface of the strain gauges before the test. In order to obtain the law of the stress signals along the axial direction, three spike teeth were selected as the measuring points, respectively located in the feeding, threshing and separating sections of this threshing cylinder. And strain gauge sensors were installed at the corresponding measuring point. The actual installation positions of each measurement point are shown in Fig.5b. In order to ensure that the signal acquisition module can work normally under the high-speed operation of the threshing cylinder, a fixing device was made using ordinary photosensitive resin material and 3D printing technology, as shown in Fig.5c.

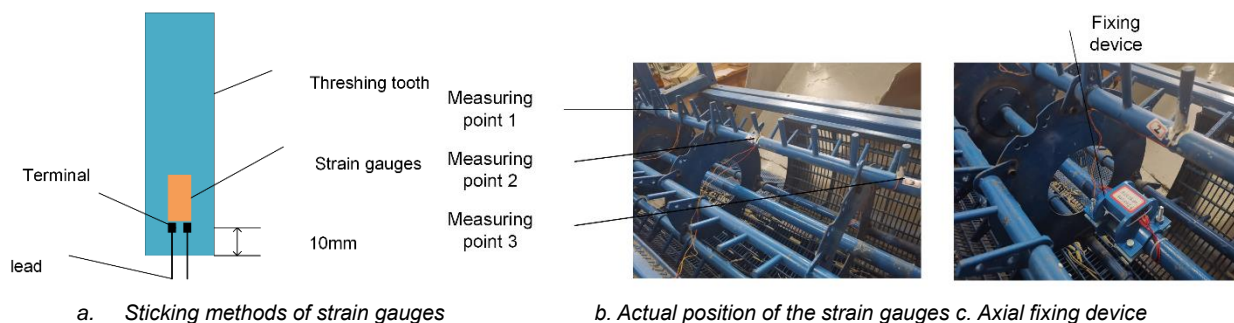


Fig. 5 - Sticking method and measuring points' position of strain gauges

The materials used in the threshing test were ripened Chinese cabbage plants harvested in the Lvyin breeding base of Jiyuan City, Henan Province, and the name of the variety was "Jincai No. 3 F1". The artificially harvested plants were randomly selected in the test field, and the threshing test was completed in time. Since the harvested Chinese cabbage plants were at the later period of the harvest, the test was completed under the condition that the moisture content of the materials was low. Measuring with a rapid moisture meter, the moisture contents of the kernels, pods and stems were 8.39%~10.26%, 13.16%~18.52%, 20.12%~25.32% respectively.

Before the vibration and impact test, the single factor and orthogonal tests of feeding rate, cylinder speed and concave clearance were carried out, and the reasonable range and optimal combination of parameters were obtained. When the feeding rate was 1 Kg/s, the cylinder speed was 750 r/min, and the concave clearance was 20 mm, the threshing unit showed the best threshing performance. With the combination of the above optimal operating parameters, the vibration and impact test bench performed the detection of the vibration and stress signals under the conditions of idling and dynamic threshing.

Before the detection of the dynamic threshing condition, to ensure a constant feeding rate of 1 Kg/s, the Chinese cabbage plants weighting 10 Kg were evenly spread on the conveyor belt with a conveying speed of 1 m/s, and five meters' acceleration adjustment zone was left.

The threshing unit, DH5902 dynamic acquisition instrument and DH5905 wireless telemetry analysis system were started at the same time. After the threshing unit started to operate stably, each channel value of the signal acquisition system was balanced and cleared, and the conveyor belt was activated. Finally, the transportation, feeding, threshing of the materials and the transmission and collection of the signals were completed. The detection under each condition was repeated 5 times, and the average data was statistically analysed to reduce the random test error.



Fig. 6 – Test site of vibration and impact detection

## RESULTS

### Detection results of the vibration

In the dynamic threshing process, the vibration signal of the axial-flow threshing cylinder was measured by a three-axis accelerometer, and the amplitude change of bearing pedestal was a time-domain process. As shown in Fig.7, it is a time-domain curve of acceleration change in the Y-direction during a complete threshing test of the axial-flow threshing unit, including the static state before the test, the startup state, the stable idling state, the dynamic threshing state, the stall state and the static state of the cylinder. It can be seen from the figure that the vibration amplitude of the bearing pedestal is significantly different under the conditions of stable idling and dynamic threshing. Fig.8 shows the vibration signals of the axial-flow threshing cylinder collected under both idling and dynamic threshing conditions.

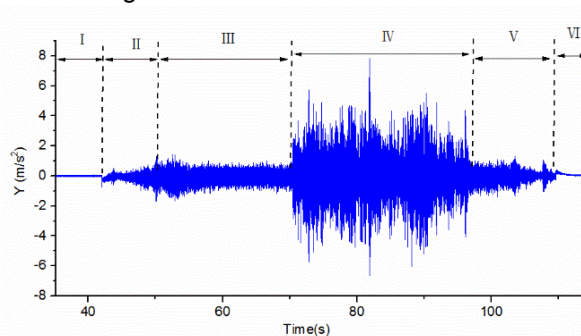


Fig. 7 - Time domain curve of the axial-flow threshing unit in one test process (Y channel)

Note: I. static; II. start; III. stable idling; IV. dynamic threshing; V. stop; VI. Static

According to the statistical results of vibration amplitude, under random vibration, the root mean square values and peak-to-peak values of the threshing process can reflect the impact of the Chinese cabbage plants on the threshing cylinder (Tang Z *et al.*, 2019). With the progress of the threshing process, the root mean square values and peak-to-peak values changed.

Part of the curves of the cylinder after stable operation under idling and threshing conditions were cut off respectively, and the root mean square value and peak-to-peak value were taken as the characteristic quantities to characterize the change of vibration signal. The vibration changes in the three directions of X, Y and Z were compared.

According to Fig. 8a and Fig. 8b, when the axial-flow threshing unit is in the idling state with no-load, the amplitude of the vibration acceleration in the X direction was  $-2.426 \sim 2.886 \text{ m/s}^2$ , and the root mean square value was  $0.757 \text{ m/s}^2$ . The peak-to-peak value was  $5.312 \text{ m/s}^2$ . However, when the materials were fed, the amplitude in the X direction increased slightly. The amplitude in X direction was  $-3.392 \sim 3.106 \text{ m/s}^2$ , the root mean square value was  $0.926 \text{ m/s}^2$ , and the peak-to-peak value was  $6.498 \text{ m/s}^2$ , increasing by 1.2 times approximately. This state of vibration in the X direction was approximately balanced.

According to Fig. 8c and Fig. 8d, the vibration amplitude significantly increased in the Y direction. The vibration amplitudes of the threshing process under no-load and dynamic threshing conditions were  $-1.027 \sim 0.917 \text{ m/s}^2$  and  $-3.896 \sim 3.792 \text{ m/s}^2$  respectively, and the root mean square values were  $0.313 \text{ m/s}^2$  and  $1.232 \text{ m/s}^2$  respectively. The peak-to-peak value was  $1.944 \text{ m/s}^2$  and  $7.688 \text{ m/s}^2$  respectively, which increased by about 4 times.

According to Fig. 8e and Fig. 8f, the vibration amplitude slightly increased in the Z direction. The vibration amplitudes of the no-load and the dynamic threshing conditions of the threshing process were  $-0.708 \sim 0.814 \text{ m/s}^2$  and  $-2.919 \sim 2.243 \text{ m/s}^2$  respectively. The root mean square values of the no-load state and the threshing state of the threshing process were  $0.236 \text{ m/s}^2$  and  $0.616 \text{ m/s}^2$ , and the peak-to-peak values were  $1.521 \text{ m/s}^2$  and  $5.234 \text{ m/s}^2$ , which increased by 2.6 times and 3.4 times respectively.

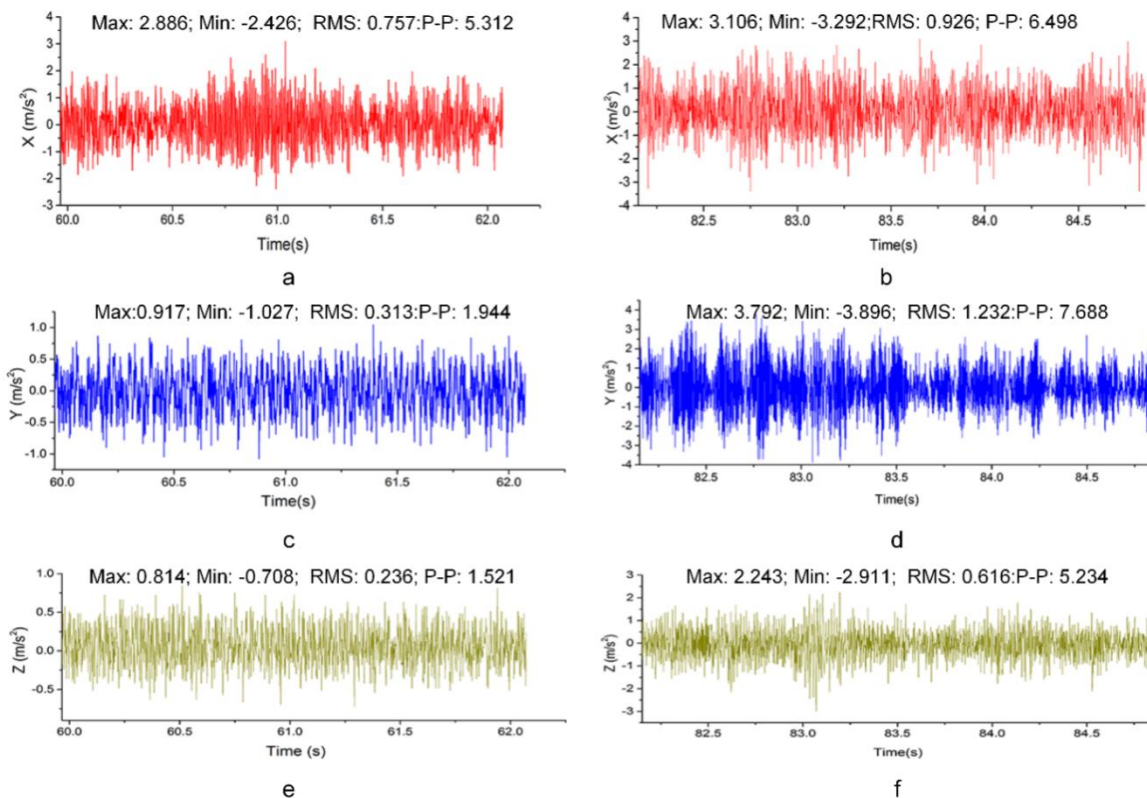


**Fig. 8 - Vibration time domain curve under idle conditions and threshing conditions in the X, Y, Z directions**

Note: Max- Maximum amplitude; Min- Minimum amplitude; RMS- root mean square; P-P- peak-to-peak

It can be seen from the above results that in the threshing process of Chinese cabbage plants, the amplitude of vibration in the X direction was slightly increased, and the change in vibration was negligible. However, the vibration amplitudes in the Y and Z directions were significantly increased. The reason for this phenomenon was that under the dynamic threshing condition, there was continuous impact and collisions between the materials and the spike teeth. The reaction force of the materials on the cylinder acted as an external excitation force, and the component forces were both in the Y and Z directions, which mainly caused the axial-flow threshing cylinder to generate a relatively strong unbalanced vibration phenomenon in the Y and Z directions, while the X direction vibration was mainly influenced by the axial force of the materials under the push of the spiral deflector and the spike teeth. The vibration in the Y direction was mainly affected by the horizontal component of the materials in the threshing cylinder.

The vibration in the Z direction was mainly caused by the vertical component of the materials in the threshing cylinder. The axial force in the X direction was significantly smaller than the forces in the Y and Z directions, which resulted in different vibration amplitudes of threshing cylinder in different directions.

**Detection results of the impact stress**

While measuring the vibration of the axial-flow threshing cylinder, the impact stress of the spike teeth in the feeding, threshing and separating sections of the threshing cylinder was detected. The results are shown in Fig.9, Fig.10 and Fig.11.

It can be seen from Fig. 9, Fig.10 and Fig.11 that the time-domain curves of the impact stress of each measuring point included three stages (taking the measuring point 1 of the feeding section as an example): the idling stage before the materials entered the cylinder, the threshing and separating stage after the materials entered the cylinder, and the idling stage after the materials stopped feeding. In the initial idling stage, the threshing cylinder was in an idling state, and the stress of every spike tooth was maintained at a value of 0; In the threshing and separating stage, the materials were continuously fed into the cylinder under the conveying of the conveyor belt. The spike tooth of each section was sequentially subjected to the materials' continuous impact and friction. The bending stress was generated inside the spike tooth, and several peak points appeared on the stress curve. In the dynamic threshing process, although the materials were fed at a constant rate, the basic size, mass, volume of the Chinese cabbage plants differed. Therefore, the spike teeth were subjected to instantaneous impacts and friction at different levels, and the peak points of stress were also at the dynamic change, so the time-domain curve was constantly changing. When the materials stopped feeding, the peak points of stress gradually decreased and eventually stabilized in the initial state or near a certain stress value. The main reason was that the materials in the cylinder were getting less and less until they were completely discharged, and the number of impact and friction of the spike teeth gradually reduced, and finally no interaction appeared anymore. At this time, the time-domain curve tended to be stable.

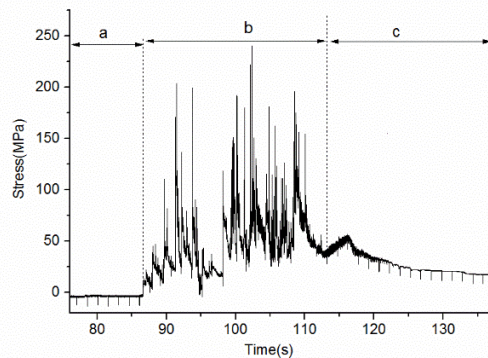


**Fig. 9 - Measuring point 1 of the feeding section**

*Note: Section a represents the idle stage before the material enters the drum, section b represents the threshing and separating stage after the material enters the cylinder, and section c represents the idle stage after the material stops feeding.*

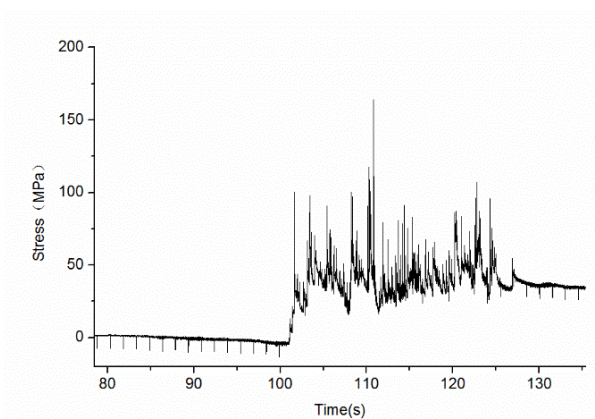


**Fig. 10 - Measuring point 2 of the threshing section**

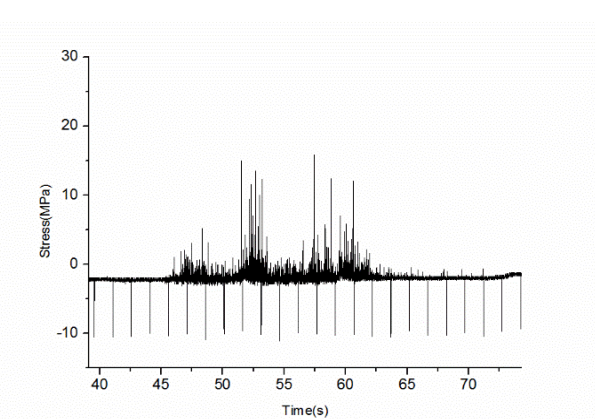


**Fig. 11 - Measuring point 3 of the separating section**

According to the analysis of the peak values of the time-domain curve of the measuring points, the peak

values of the stress in the feeding section, the threshing section and the separating section decreased in turn. Among them, the stress peak value of the feeding section was the largest and the curve was the most intensive.

The maximum value was 240.575 MPa, and the peak points spread around 200 MPa, as shown in Fig.9. The stress peak value of the threshing section spread around 90 MPa, and the maximum value was 164.128 MPa, as shown in Fig.10. The stress peak value of the separating section was smaller, and the maximum stress peak was only 15.835 MPa, as shown in Fig.11. The reason for this phenomenon was that in the feeding section, the materials were relatively concentrated, which means the volume and weight of the materials were large, so the impact of the spike teeth was strong, resulting in a large internal bending stress. When entering the threshing section, most of the materials were threshed and separated, and some stalks and seeds were removed and separated into the receiving device through the concave sieve. As the material layer became thinner, the volume and mass of the materials decreased, which led to the decrease of the impact on the spike teeth, and the stress generated inside. Similarly, with the process of threshing and separating, there were fewer materials entering the separating area. In addition to the impact of a small amount of materials, there was more friction between the spike tooth and the materials. Therefore, the stress peak value was the lowest, and the time-domain curve was less intensive.

Fig.12 showed the local curve of the dynamic stress of the spike tooth changing from the idling state to the threshing state. It can be seen from the figure that before the materials were fed in, due to the influence of the vibration of the machine, the rotation speed of the cylinder and the self-weight of the spike tooth, the stress peak points of the spike tooth appeared at equal intervals. The values of the three sections were -13.412 MPa, -13.412 MPa, -11.119 MPa respectively. When contacting with the materials, the stress value of the spike tooth instantly rose to the peak, and then gradually decreased until the next collision occurred. And the next peak point appeared. During the time  $t_i$  when the material contacted with the spike tooth, because the mass of the materials and the speed difference between them were the largest, the stress generated in the tooth was also the largest. With the contact action, the speed difference between the spike tooth and the materials continuously decreased, and the materials' quality also gradually decreased with the threshing process. After the impact, the friction force decreased gradually, and the bending stress generated by the spike tooth also decreased. This phenomenon is consistent with the derivation of Equation 2. Each subsequent impact is a repetition of the above process.

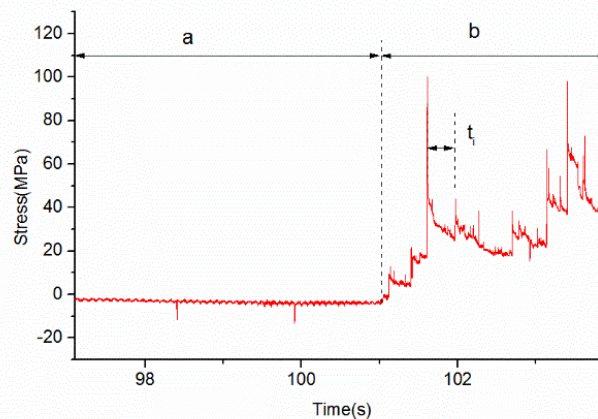


**Fig. 12 - Local stress time-domain curve from idling to threshing state.**

*Note:  $t_i$  is the contact time of the materials and the spike tooth during a collision*

## CONCLUSIONS

1. With the change of axial-flow threshing unit from idling to dynamic threshing condition, the amplitude in the X direction increases from  $-2.226\sim 2.86$  m/s<sup>2</sup> to  $-3.392\sim 3.106$  m/s<sup>2</sup>. The root mean square value changes from 0.757 m/s<sup>2</sup> to 0.926m/s<sup>2</sup>. The peak-to-peak value changes from 5.312 m/s<sup>2</sup> to 6.498 m/s<sup>2</sup>. The amplitude in the Y direction increased from  $-1.027\sim 0.917$  m/s<sup>2</sup> to  $-3.896\sim 3.792$ m/s<sup>2</sup>. The root mean square value increases from 0.313 m/s<sup>2</sup> to 1.232 m/s<sup>2</sup>. The peak-to-peak value changes from 1.944 m/s<sup>2</sup> to 7.688m/s<sup>2</sup>.

The amplitude in the Z direction increases from  $-0.708\sim 0.814$  m/s<sup>2</sup> to  $-2.919\sim 2.243$  m/s<sup>2</sup>, and the root mean square value increases from 0.236 m/s<sup>2</sup> to 0.616 m/s<sup>2</sup>, and the peak-to-peak value changes from 1.521 m/s<sup>2</sup> to 5.234 m/s<sup>2</sup>.

The change of the vibration state in the X direction was so small that can be ignored, but the change of amplitude in the Y and Z directions were obvious, which were mainly caused by the components of the impact load between the threshing cylinder and materials.

2. Under continuous and stable dynamic threshing condition, the values of impact stress of spike teeth in different sections are as follows: the peak value of the stress in the feeding section is the largest, concentrated at about 200 MPa; The threshing section is the second, concentrated at about 90 MPa; The maximum peak value of the separating section is only about 15 MPa. The peak values of impact stress of the separating section are the most intensive, because the stress of the feeding and threshing section is mainly determined by the impact force, while the separating section is affected by a small amount of materials' impact and a large amount of friction.

3. In a very short period of contact between the materials and the spike tooth, the stress values generated by the spike tooth at each measuring point first appears the peak value and then gradually decreases until the next impact point appears. The magnitude and change trend of the stress peak value is mainly determined by the quality and speed of the materials.

## ACKNOWLEDGEMENT

This work was sponsored by the National Key Research and Development Program (2017YFD0701204) and National Innovation and Entrepreneurship Training Program for College Students (10464009).

## REFERENCES

- [1] Bello B., Tokan A, Jiya D. et al, (2019), Design Model of Automated Groundnut Threshing Machine, *Majlesi Journal of Mechatronic Systems*, Vol.8, Issue1, pp.19-24, Abubakar Tafawa Balewa/Nigeria.
- [2] Chansrakoo W, Chuan-Udom S, (2018), Factors of Operation Affecting Performance of a Short Axial-flow Soybean Threshing Unit, *Engineering Journal*, Vol.22, Issue4, pp.109-120, KhonKaen / Thailand.
- [3] Li Yaoming, Ye Xiaotian, Xu Lizhang et al, (2013), Construction and performance experiment of load test system for half axle of combine harvester, *Transactions of the Chinese Society of Agricultural Engineering (Transactions of the CSAE)*, Vol.29, Issue 6, pp.35-41, Jiangsu /China.
- [4] Miu P., Kutzbach H., (2008), Modeling and simulation of grain threshing and separation in threshing units-Part I, *Computers and Electronics in Agriculture*, Vol.60, Issue 1, pp.96-104, Tennessee/ United States.
- [5] Syuhri A, Sholahuddin I, Syuhri S., et al, (2018), Modeling and evaluation of a threshing drum under vertical vibration, *Journal of Mechanical Engineering and Sciences*, Vol.12, Issue 2, pp. 3750-3758, Jember/Indonesia.
- [6] Steponavicius D, Puzauskas E, Spokas L, et al, (2018), Concave Design for High-Moisture Corm Ear Threshing. Mechanics, *Design and Optimization of Mechanical Systems*, Vol.24, Issue 1, pp. 80-91, Akademija/Lithuania.
- [7] Tang Zhong, Zhang Haotian, Zhou Yuepeng, et al, (2019), Mutual Interference and Coupling Response of Multi-cylinder Vibration among Combine Harvester Co-Frame, *Impact and Vibration*, Vol.2019, pp.1-14, Jiangsu/China.
- [8] Tang Zhong, Li Yaoming, Wang Chenghong, (2013), Experiments on Variable-mass Threshing of Rice in the Tangential-longitudinal-flow Combine Harvester, *Jomo Kenyatta University of Agriculture and Technology*, Vol.15, pp.1319-1334, Jiangsu/China.
- [9] Wang Yue, Ma Ji, (1987), Research on principle of grain threshing and straw breaking in the axial-flow threshing apparatus, *Transactions of the Chinese Society for Agricultural Machinery*, Issue 1, pp. 57-91, Beijing/China.
- [10] Xie Fangfei, Luo Xiwen, Lu Xiangyang, et al, (2009), Kinetic analysis of flexible threshing under law of conservation of energy. *Journal of Hunan Agricultural University (Natural Sciences)*, Vol.35, Issue 2, pp.181-184, Hunan/China.
- [11] Zare H., Maleki A., Rahaghi M., et al, (2019), Vibration modelling and structural modification of combine harvester thresher using operational modal analysis and finite element method, *Structural Monitoring and Maintenance*, Vol.6, Issue 1, pp. 33-46, Islamic/Iran.